Supplementary Online Materials (SOM) for

Morphometric analysis of the hominin talus: Evolutionary and functional implications

This file includes:

SOM Section 1. Individual facets.

1.1 Medial malleolar facet

Shape variability of the medial malleolar facet (Fig. S2a,d,e) shows a degree of overlap between African apes and *H. sapiens*, suggesting that the morphology of this facet is not useful when interpreting locomotor behaviour of fossil hominins. The latter falls mainly within *Pan* and, to a lesser extent, into the *H. sapiens* range of variability. Only TM 1517 (*P. robustus*) plots in the *Gorilla* range of variation. PC1 (31.9%) accounts for significant differences among all three extant groups (ANOVA, Df = 2, *F*-test = 94.7, *p* = < 0.001, Table S4) and shape changes recorded on it correlate with lnCS (r = 0.1673, *p* = 0.0338). Morphological dissimilarity expressed along PC2 (23.2%) and PC3 (13.1%) significantly correlates with lnCS measured in both (r = -0.2717, *p* = 0.0004 and r = -0.4059, *p* = < 0.001 respectively). *Gorilla* and *H. sapiens* significantly differ from *Pan* along PC2 (ANOVA, Df = 2, *F*-test = 15.1, *p* = < 0.001, Table S4) and PC3 (ANOVA, Df = 2, *F*-test = 37.1, *p* = < 0.001, Table S4).

Shape change along axes reflects a general pattern shared by all three PCs exhibiting variation in convexity and expansion of the distal border of the facet (Fig. S2c).

The first three form space PCs explain 79.7% of overall variance (Fig. S2b), showing the same overlap between extant taxa as in shape space, with fossil hominins falling in this overlapping area. Even if the trajectories of extant groups are not parallel in the plot, neither angles nor magnitudes were found to significantly differ between pairs of extant groups.

1.2 Anterior-medial calcaneal facet

Similarly, the anterior-medial calcaneal facet of extant samples overlaps in the shape space PCA (Fig. S3a,d,e), suggesting that the anterior calcaneal facet is not helpful in discriminating bipedal from quadrupedal forms. Post hoc ANOVA reveals that PC1 (30.5%) accounts for significant differences between *Gorilla* and *Pan,* as well as *H. sapiens* and *Pan* (ANOVA, Df = 2, *F*-test = 17.6, *p* = < 0.001, Table S4). PC2 (20.1%) differentiates *H. sapiens* from African apes (ANOVA, Df = 2, *F*-test = 66.8, *p* = < 0.001, Table S4), while PC3 (15.8%) accounts for differences between *Pan* and *H. sapiens* (ANOVA, Df = 2, *F*-test = 3.9, *p* = 0.0213, Table S4).

Shape change ranges from rounded and extended dorsally (PC1 negative) to a flatter and relatively expanded antero-posteriorly facet (PC1 positive) (Fig. S3c). Positive values on PC2 reflect flatter articular facet, while PC2 negative values indicate a more convex shape, with the anterior facet perpendicularly oriented in respect to the medial facet. Extreme positive values on PC3 reflect flatter and larger anterior-medial calcaneal facets, while an antero-posterior narrowed and spherical surface occupies the negative extreme on the same axis. Shape divergence between *Pan* and *H. sapiens* in PC3 is also related to differences in lnCS (r = -0.1968, p = 0.0141).

Form space (Fig. S3b) shows fossil hominins falling in the area of overlap between extant groups in the first three PCs (77.7%). No significant differences in angle or magnitude of allometric trajectories were found.

SOM Section 2. Combined facets.

2.1 Talocrural joint

The talar structures associated with the talocrural joint were assessed combining the trochlea with 1) the lateral malleolar facet, 2) the medial malleolar facet, and 3) both the lateral and medial malleolar facets. These three combinations are the only ones that exhibit slight overlap between the ranges of extant hominins.

2.1.1 Combined trochlea and lateral malleolar facet In shape space (Fig. S4a,d,e), PC1 (27.9%) tends to separate African apes from *H. sapiens* (ANOVA, Df = 2, F-test = 220.5, p = < 0.001, Table S4), with less clear separation between australopiths and early non-*erectus Homo* (plotting between *Pan* and *H. sapiens*) from extinct *Homo* (close to or falling inside the *H. sapiens* range). Interestingly, StW 486 (*A. africanus*) plots close to late extinct *Homo* and falls inside the *H. sapiens* range. PC1 negative values exhibit a trapezoidal trochlea with an elevated lateral rim accompanied by a more laterally extended and curved lateral surface. On the other hand, PC1 positive values are characterized by a relatively more flat and large trochlea with a less laterally extended lateral surface (Fig. S4c). PC2 (12.2%) accounts for significant differences among all

three extant groups (ANOVA, Df = 2, *F*-test = 70.9, *p* = < 0.001, Table S4). PC2 positive values display a relatively deeper trochlear groove, medial extension of the posterior margin and anteriorly oriented lateral facet when compared to PC2 negative (Fig. S4c). No significant differences were found among taxa in PC3 (ANOVA, Df = 2, *F*-test = 1.7, *p* = 0.181, Table S4), which only accounts for 9% of overall variation. PC3 seems to reflect a change in medial extension of the lateral malleolar facet (Fig. S4c). The three PCs are correlated with lnCS (PC1, r = 0.3134, *p* = < 0.001; PC2, r = -0.4316, *p* = < 0.001; PC3, r = 0.2310, *p* = 0.0032). The three form space PCs account for 76.9% of overall variance (Fig. S4b). While PC1 segregates *Gorilla* and *H. sapiens* from *Pan*, PC2 and PC3 separate African apes from *H. sapiens*. Australopiths are closer to *Pan* trajectories than are other fossil hominins, which are closer to *H. sapiens* trajectories or fall between African apes and *H. sapiens*. *Pan* shows a different allometric trajectory from *H. sapiens* (α = 14, *p* = 0.0159) and *Gorilla* (α = 19.8, *p* = 0.0009; magnitude *p* = 0.0299).

2.1.2 Combined trochlea and medial malleolar facet In shape space (Fig. S5a,d,e), PC1 (32.4%) accounts for significant differences between African apes and *H. sapiens* (ANOVA, Df = 2, *F*-test = 191.8, *p* = < 0.001, Table S4) with only small overlap between African apes and *H. sapiens*. A trapezoidal and grooved trochlea with a cupped medial facet (PC1 negative values) separates African apes from *H. sapiens*, which exhibit a flat and squared trochlea with a flat medial facet instead (PC1 positive values; Fig. S5c). Most of the australopiths, early non-*erectus Homo*, and *H. naledi* fall inside or just outside the observed range of *Pan* variability, while other fossil *Homo* specimens fall closer to the range of observed *H. sapiens* variability. StW 486 (*A. africanus*) and StW 363 (*A. africanus*) are exceptions, however, since they fall inside the *H. sapiens*, whereas StW 88 falls inside the *Pan* range. As in the case of the trochlea, we compared phenetic distance measured among specimens of *A. africanus* with those of extant taxa. Results (Fig. S6) show a comparatively larger distance exhibited by *A. africanus* than exhibited by *H. sapiens* (*p* = < 0.05), but not as large as the random distances exhibited by *Pan* and to a markedly lesser extent by *Gorilla.* Shape space PC2 (12%) shows significant differences among all three extant groups (ANOVA, Df = 2, *F*-test = 103.6, *p* = < 0.001, Table S4) and is negatively correlated with lnCS

(r = -0.5797, *p* = < 0.001), while PC3 (8.9%) discriminates *Pan* from *Gorilla* (ANOVA, Df = 2, *F*-test = 3.4, *p* = 0.033, Table S4). PC2 negative and PC3 positive values display an antero-posterior extension of the trochlea resulting in a rectangular shape compared to the shorter and trapezoidal trochlea along PC2 positive and PC3 negative. More cupped medial malleolar facets are also assigned negative values on PC2 and positive values on PC3 (Fig. S5c). In form space, the allometric trajectory of *Pan* differs from that of *H. sapiens* (α = 16.7, *p* = 0.0089; magnitude *p* = 0.0119) and *Gorilla* (α = 24.2, *p* = 0.0019; magnitude *p* = 0.0099). Australopiths, *H. habilis*, *H. naledi* and *H. floresiensis* appear to follow the trajectory of *Pan*, while other fossil *Homo* specimens are placed around the *H. sapiens* trajectory.

2.1.3 Combined trochlea, lateral and medial malleolar facets As already documented for the combination of the trochlea with lateral and medial facets, respectively, shape space PCA (Fig. S7a,d,e) shows that australopiths (with the exception of StW 486 and StW 363), early non-*erectus* *Homo,* and *H. naledi* plot next to *Pan*, while other extinct *Homo* plot closer to the *H. sapiens* range. PC1 (29.6%) discriminates between African apes and *H. sapiens* (ANOVA, Df = 2, *F*-test = 262.3, *p* = < 0.001, Table S4) based on the difference between a grooved and trapezoidal trochlea coupled with flared medial and lateral facets that characterize African apes versus a squared, flat trochlea and lateral facet that characterize *H. sapiens* (Fig. S7c). PC2 (12%) shows differences among all three extant groups (ANOVA, Df = 2, *F*-test = 116, *p* = < 0.001, Table S4), while PC3 (8%) does not exhibit any significant difference among groups (ANOVA, Df = 2, *F*-test = 1.9, *p* = 0.141, Table S4). Morphological change along PC2 is the same as described before (Figs. S4 and S5). All three PCs correlate with lnCS (PC1, r = 0.3013, *p* = 0.0001; PC2, r = -0.5180, *p* = < 0.001; PC3, r = 0.2374, *p* = 0.0024). Form space PCA (Fig. S7b) yields similar results to those obtained for the combination of the trochlea and medial malleolar facet. In this case, however, a significant difference was found between the allometric trajectories of *Pan* and *Gorilla* (α = 17.8, *p* = 0.0009; magnitude *p* = 0.0379).

In summary, the same patterns characterizing the fossil hominin distribution are recognizable in the combined trochlea and medial malleolar facet (Fig. S4) and in the combined trochlea, lateral

and medial malleolar facets (Fig. S5), suggesting a primitive retention in the geometric configuration of these combinations in australopiths and early non-*erectus Homo.*

2.2 Talocrural and subtalar joints

The relationship between talocrural and subtalar joints was explored analysing the combination of the posterior calcaneal facet, trochlea, and the medial and lateral malleolar facets (Fig. S8), and the combination of the posterior calcaneal facet and trochlea (Fig. S9). Both combinations yielded a relatively clean separation between African apes and *H. sapiens*.

2.2.1 Combined posterior calcaneal facet, trochlea, medial and lateral malleolar facets In shape space (Fig. S8a,d,e), PC1 (29%) separates African apes from *H. sapiens* (ANOVA, Df = 2, *F*-test = 576.1, $p = < 0.001$, Table S4), with StW 88 (*A. africanus*) and KNM-ER 1476 (*Homo* spp./ *P. boisei*) plotting close to the African ape range, U.W. 88-98 (*A. sediba*) and A.L. 288-1 (*A. afarensis*) plotting between African apes and *H. sapiens*, StW 363 (*A. africanus*) plotting next to *H. sapiens*, and fossil *Homo* specimens plotting close to or inside the range of *H. sapiens* variability. PC2 (9.3%) accounts for significant differences among all three extant groups (ANOVA, Df = 2, *F*-test = 65.6, $p = < 0.001$, Table S4), while PC3 (7.1%) discriminates between *Pan, Gorilla* and *H. sapiens* (ANOVA, Df = 2, *F*-test = 8.1, $p = 0.0004$, Table S4). Morphological change in the first three PCs correlates with lnCS (PC1, r = 0.4777, $p = < 0.001$; PC2, r = 0.4480, $p = 0.0003$; PC3, r = -0.1983, $p = 0.0091$). PC1 negative exhibit a more concave posterior calcaneal facet, a trapezoidal and grooved trochlea, and flared lateral malleolar facets compared to PC1 positive (Fig. S8c). Shapes along positive PC2 and PC3 are characterized by a relatively flatter trochlea, a flatter posterior calcaneal facet, and a less concave lateral facet. Form space PCA (Fig. S8b) separates *Gorilla* and *H. sapiens* from *Pan* along PC1 (66.6%), and African apes from *H. sapiens* on PC2 (8%). The *Pan* trajectory is significantly different to that of *H. sapiens* ($\alpha = 11.7$, $p = 0.0459$; magnitude $p = 0.0069$) and *Gorilla* ($\alpha = 12.4$, $p = 0.0269$; magnitude $p = 0.0189$). Australopiths are closer to *Pan*, while other fossil hominins are closer to the trajectory of *H. sapiens*.

2.2.2 Combined posterior calcaneal facet and trochlea Results from shape and form space are similar to those of the combined posterior calcaneal facet, trochlea, and the medial and lateral malleolar facets. The distribution of fossil hominins, however, is clearer in the present case. In shape space (Fig. S9a,d,e), significant differences are present in the distribution of values along PC1 (29.9%), which distinguishes African apes from *H. sapiens* (ANOVA, Df = 2, *F*-test = 457.5, $p = < 0.001$). *A. afarensis* (A.L. 288-1), *A. africanus* (StW 88), *A. sediba* (U.W. 88-98) and KNM-ER 1476 (*Homo* spp./ *P. boisei*), followed by StW 363 (*A. africanus*), are closer to the range associated with African apes. Fossil *Homo* specimens fall close to or within the range of *H. sapiens* variability. Shape of the talus changes from a trapezoidal and sloping trochlea with a relatively more concave posterior calcaneal facet (PC1 negative) to essentially a squared and flatter trochlea and a less concave posterior calcaneal facet (PC1 positive) (Fig. S9c). PC3 (8.1%) accounts for differences among all extant taxa (ANOVA, Df = 2, *F*-test = 64.2, $p = < 0.001$, Table S4), while no significant values have been found for PC2 (ANOVA, Df = 2, *F*-test = 0.4, $p = 0.635$, Table S4), which explains 9% of overall variation. Both PC1 ($r = 0.4823$, $p = < 0.001$) and PC3 ($r = -0.4389$, $p = < 0.001$) correlate with lnCS.

The three form space PCs explain 78% of overall variance (Fig. S9b). *Gorillas* and *H. sapiens* differ from *Pan* in PC1 (66.6%), while African apes are separated from *H. sapiens* in PC2 (8%). *Gorilla* and *Pan* trajectories differ in angle and magnitude ($\alpha = 11.7$, $p = 0.0449$; magnitude $p = 0.0189$), while *H. sapiens* are different from *Pan* in magnitude only ($p = 0.0039$). Smaller specimens (australopiths, *H. habilis*, *H. naledi*, *H. floresiensis*) and KNM-ER 1476 (*H. erectus*) plot next to *Pan*, while larger (bodied) specimens are closer to *H. sapiens*.

2.3 Transverse, talocrural and subtalar joints

Being a component of the transverse tarsal joint, the navicular facet was associated in turn with the posterior calcaneal facet and trochlea.

2.3.1 Combined navicular and posterior calcaneus facets The combined navicular and posterior calcaneus facets (Fig. S10a,d,e) distinguish African apes from *H. sapiens* in shape space (ANOVA, Df = 2, *F*-test = 371.4, $p = < 0.001$, Table S4) along PC1 (35.6% of total variance).

PC1 negative reflects flatter, larger head with a reduced distance from the posterior calcaneus compared to PC1 positive (Fig. S10c). Fossil hominins are intermediate between extant taxa, with the exception of *A. sediba* (U.W. 88-98), which falls inside the range of *Pan*, and a few Neandertals and one *H. naledi* talus that all fall within the range of *H. sapiens* variability. *A. afarensis* (A.L. 288-1), *A. africanus* (StW 88) and Dmanisi (D4110) exhibit more ape-like relationships between the navicular and posterior calcaneal facets. PC2 (8.9%) represents differences between *Pan* and both *H. sapiens* and *Gorillas* (ANOVA, Df = 2, *F*-test = 7.6, *p* = 0.0006, Table S4). Shape changes from rounded navicular facets with a more concave posterior calcaneal facet plotting close to negative values on PC2 to a flatter, more rectangular navicular facet with a less concave posterior facet plotting close to positive values (Fig. S10c). Both PC1 and PC2 correlate with lnCS (PC1, r = -0.3188, *p* = < 0.001; PC2, r = -0.2829, *p* = 0.0003). PC3 (7.8%) shows no significant differences among extant taxa (ANOVA, Df = 2, *F*-test = 0.8, *p* = 0.419). The three form space PCs account for 81.9% of overall variance. While PC1 accounts for differences in lnCS, PC2 tends to separate African apes from *H. sapiens*. Modern humans are different from *Pan* in magnitudes of their allometric trajectory (P = < 0.05), but not in the angle. Fossil hominins plot between *Pan* and *H. sapiens*, except for Neandertals, which plot inside the range of *H. sapiens* variability.

2.3.2 Combined navicular facet and trochlea With the combined navicular facet and trochlea (Fig. S11a,d,e), we obtained a clearer separation among fossils than the one obtained through the previous combination of features (Fig. S9). Shape space PC1 (40.6%) discriminates *H. sapiens* from African apes (ANOVA, Df = 2, *F*-test = 574.4, *p* = < 0.001, Table S4). *Australopithecus africanus* (StW 88) and *A. sediba* (U.W. 88-98) are the hominins that plot closest to the ranges of African apes, but *H. habilis* (OH8) and D4110 are also quite close. *Australopithecus afarensis* (A.L. 288-1) is the only species of *Austraopithecus* wherein the talus plots close to the *H. sapiens* range, while more recent hominin species (one *H. naledi*, *H. floresiensis* and Neandertals; Fig. S10a) also do. PC1 positive show that the navicular facet is more centrally displaced and downward oriented with respect to the trochlea, in addition the trochlea and the navicular facets are flatter than those represented PC1 negative (Fig. S10c). PC2 (8.7%) shows differences between *Pan* and *Gorilla* (ANOVA, Df = 2, *F*-test = 4.3, *p* = 0.0143,

Table S4). PC2 negative values exhibit larger surfaces and a less dorsally extended navicular facet compared to PC2 positive values (Fig. S11c). For PC3 (6.4%), no significant differences were found (ANOVA, Df = 2, *F*-test = 0.8, *p* = *0.*419). PC1 and PC2 are correlated with lnCS (PC1, r = 0.4584, *p* = < 0.001; PC2, r = 0.1851, *p* = 0.021). The three form space PCs account for 83% of overall variance (Fig. S11b). PC1 (67.7%) reflecting differences in lnCS, while PC2 (11.2%) separates African apes from *H. sapiens*. *Australopithecus afarensis* seem to follow the *H. sapiens* trajectory, while *A. africanus*, *A. sediba*, and *H. habilis* are closer to the trajectory of *Pan*. No differences in angles and magnitudes of allometric trajectories are present among extant groups.

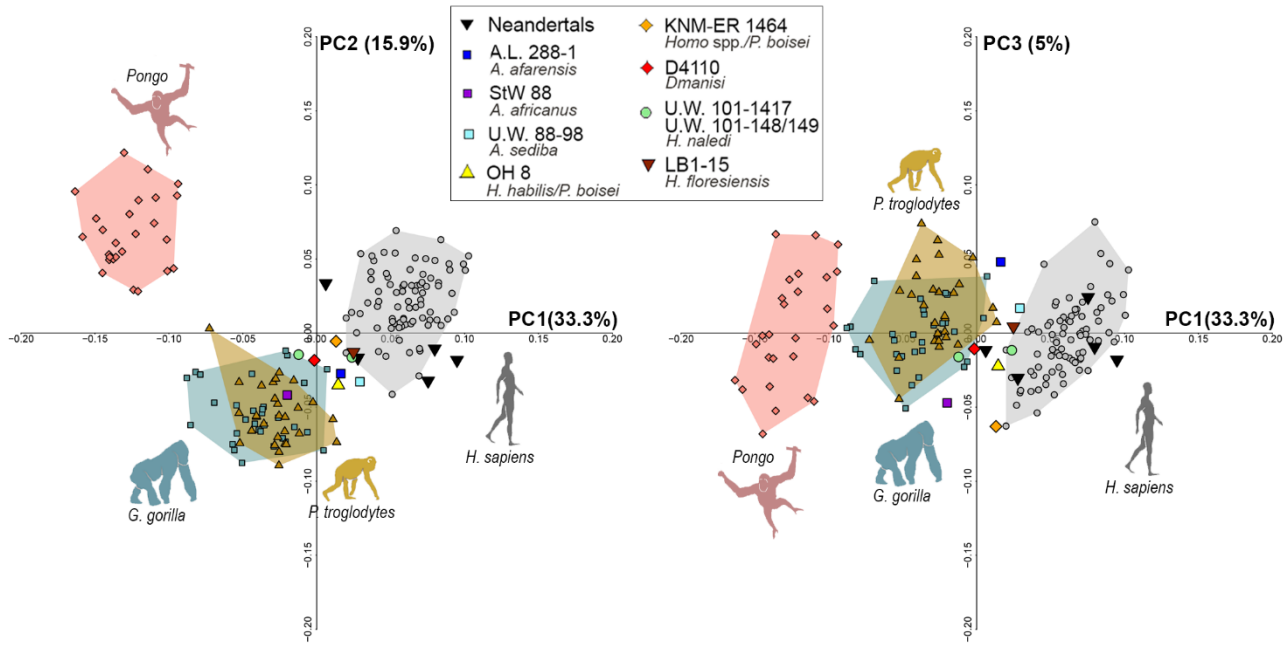

Fig. S1. Shape space PCA plots (PC1-PC2 on the left; PC1-PC3 on the right) of the whole talus including *Pongo (P. pygmaeus* and *P. abelii)*. The *Pongo* sample is housed at Zoologische Staatssammlung München, Munich and National Museum of Natural History, Smithsonian, Washington. Comparing this plot with that in Figures 4a-5, it is evident that when *Pongo* is included the morphospace change minimizing the differences between *Pan* and *Gorilla.* Fossil hominins plot between African apes and *H. sapiens*, therefore we decided do not to include *Pongo* in the present work.

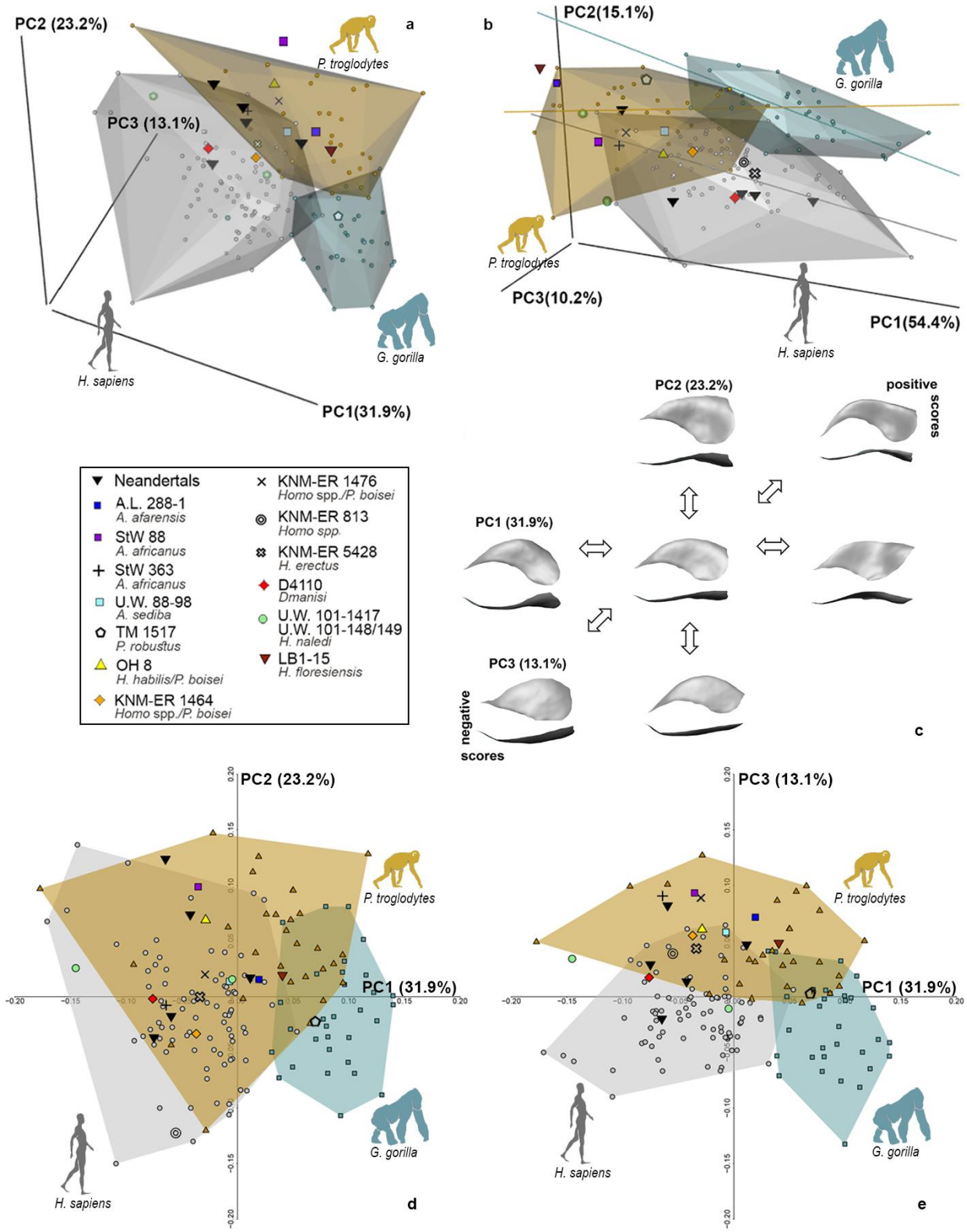

Fig. S2. Medial malleolar facet. 3D PCA plot in shape space (**a**) and form space (**b**). Shape changes of the medial malleolar facet along the first three shape PCs (**c**) in medial (above) and dorsal (down) views. 2D PCA depicting PC1 vs. PC2 (d) and PC1 vs. PC3 (e).

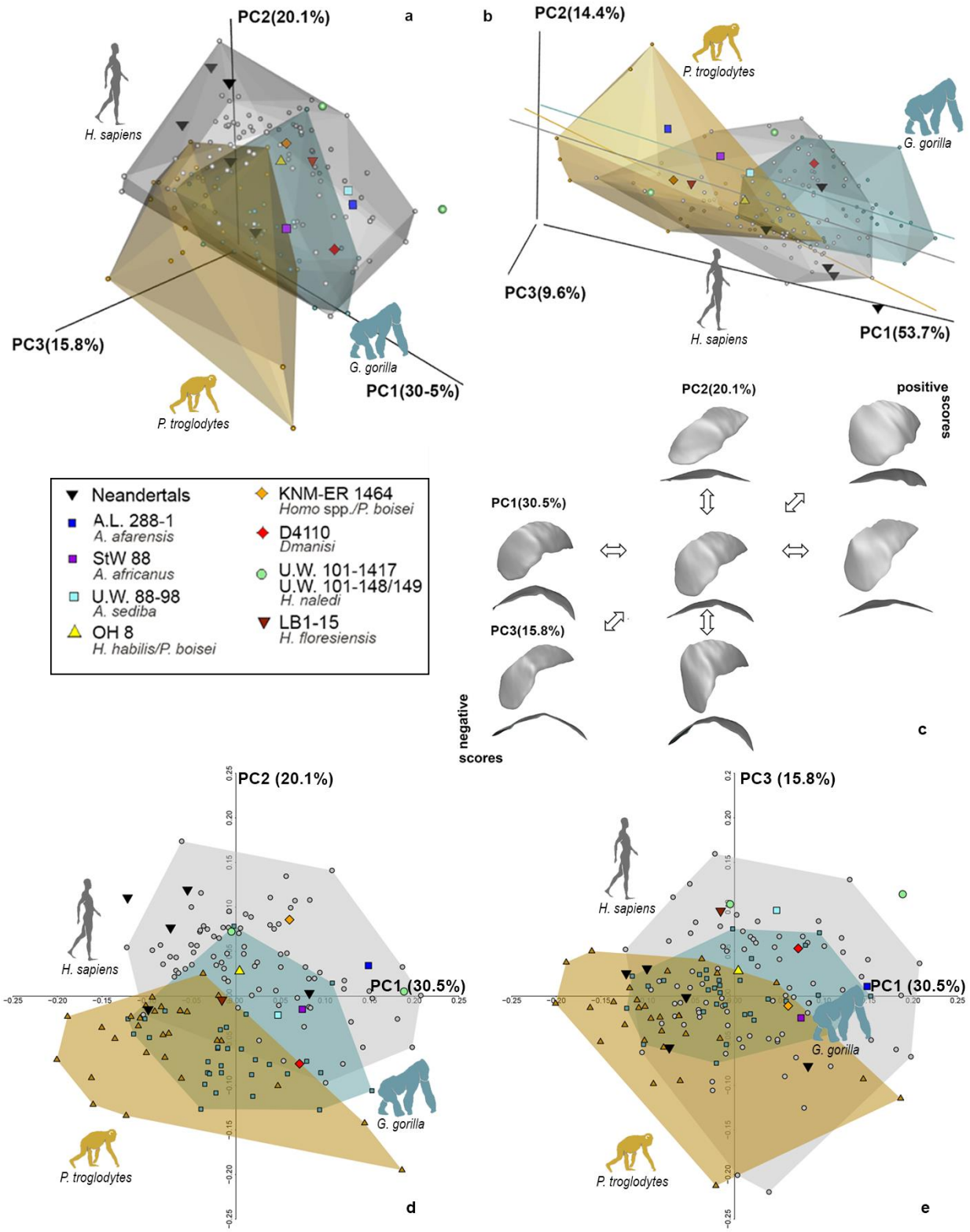

Fig. S3. Anterior-medial calcaneal facet. 3D PCA plot in shape space (**a**) and form space (**b**). Shape changes of the anterior-medial calcaneal facet along the first three shape PCs (**f**) in plantar (above) and posterior (below) views. 2D PCA depicting PC1 vs. PC2 (d) and PC1 vs. PC3 (e).

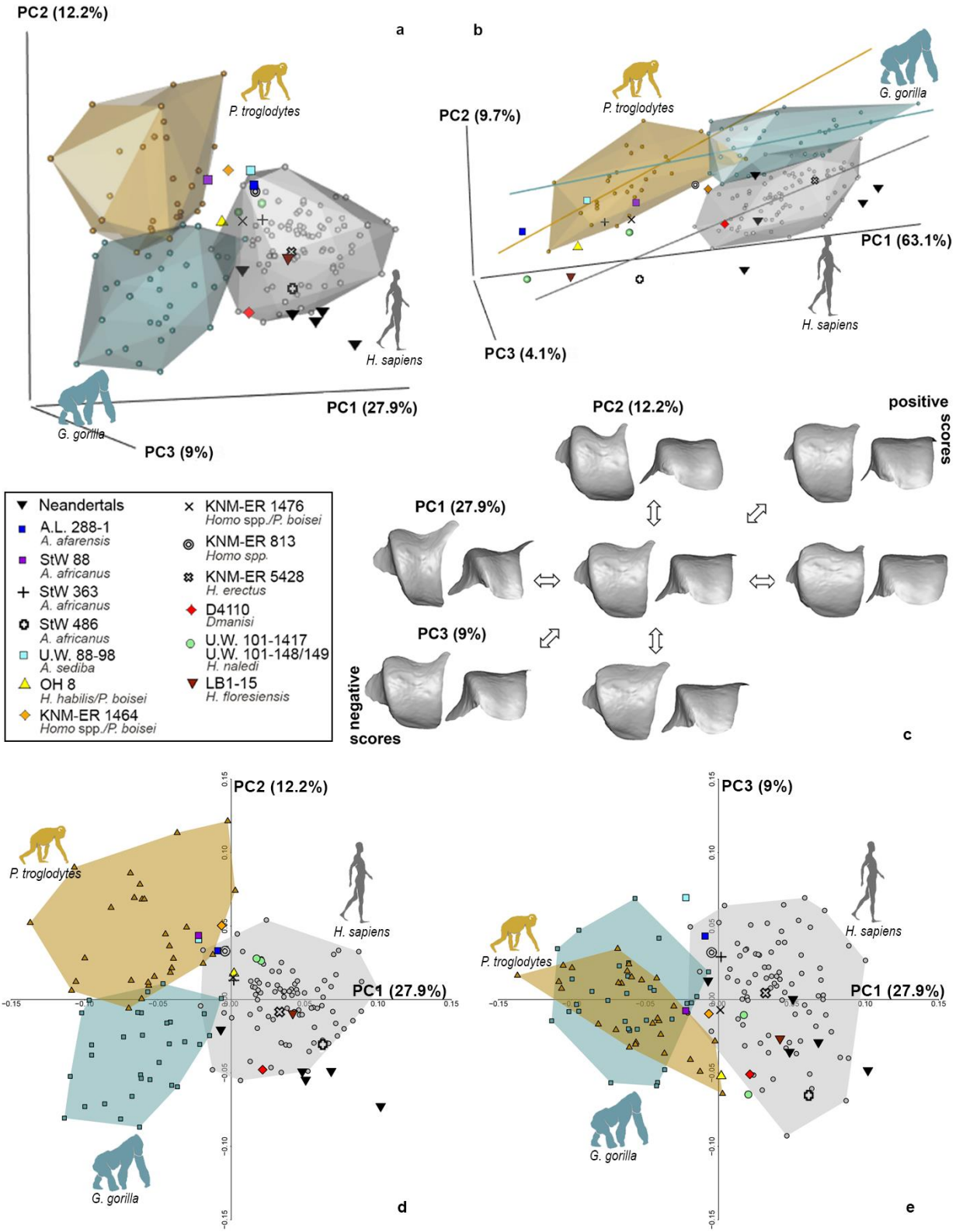

Fig. S4. Combined trochlea and lateral malleolar facet. PCA plot of the trochlea and lateral malleolar facet in shape space (a) and in form space (b). Shape changes along the first three PC axes (c) in dorsal (left) and posterior (right) views. 2D PCA depicting PC1 vs. PC2 (d) and PC1 vs. PC3 (e).

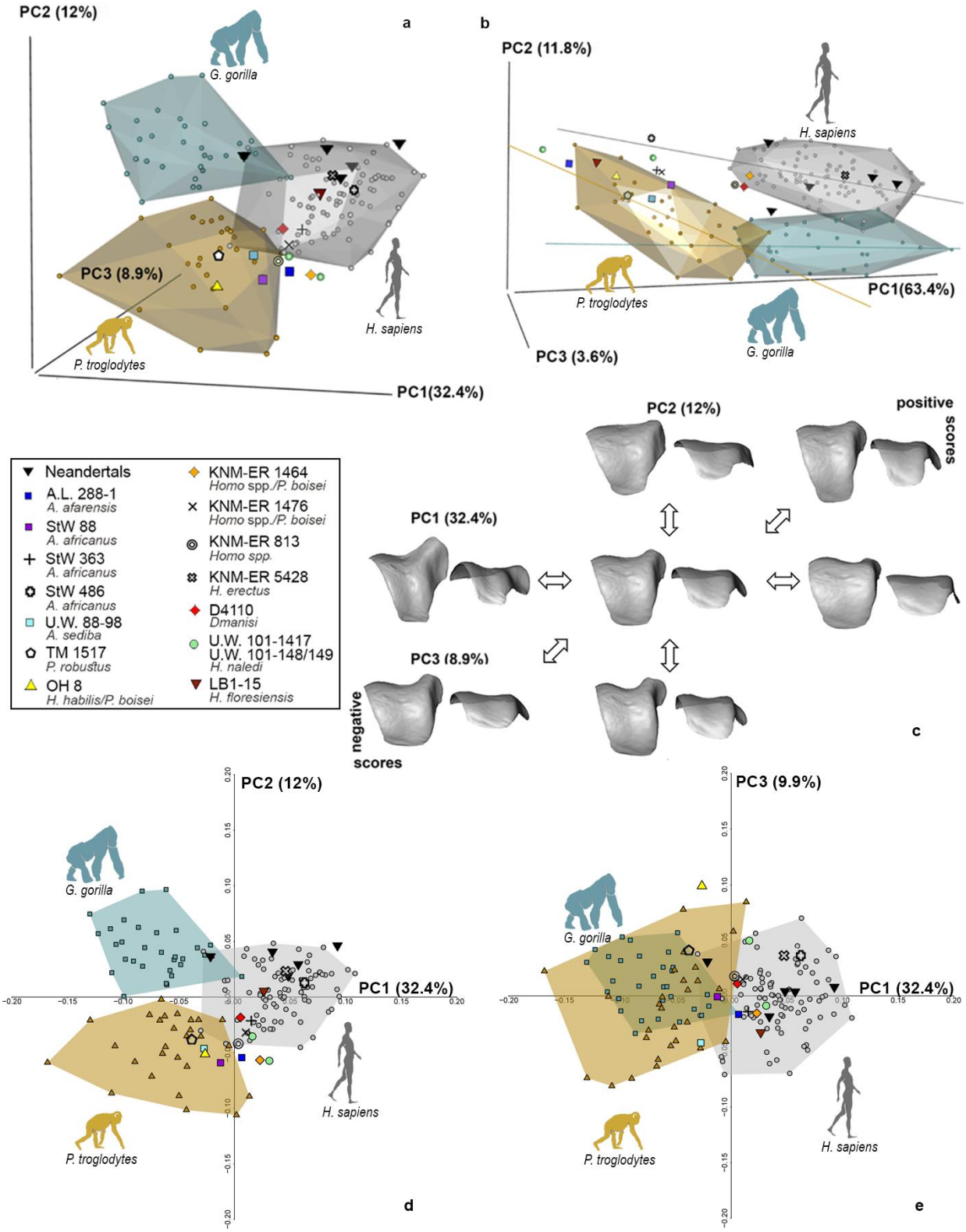

Fig. S5. Combined trochlea and medial malleolar facet. PCA plot of the trochlea and medial malleolar facet in shape space (a) and in form space (b). Shape changes along the first three PC axes (c) in dorsal (left) and posterior (right) views. 2D PCA depicting PC1 vs. PC2 (d) and PC1 vs. PC3 (e).

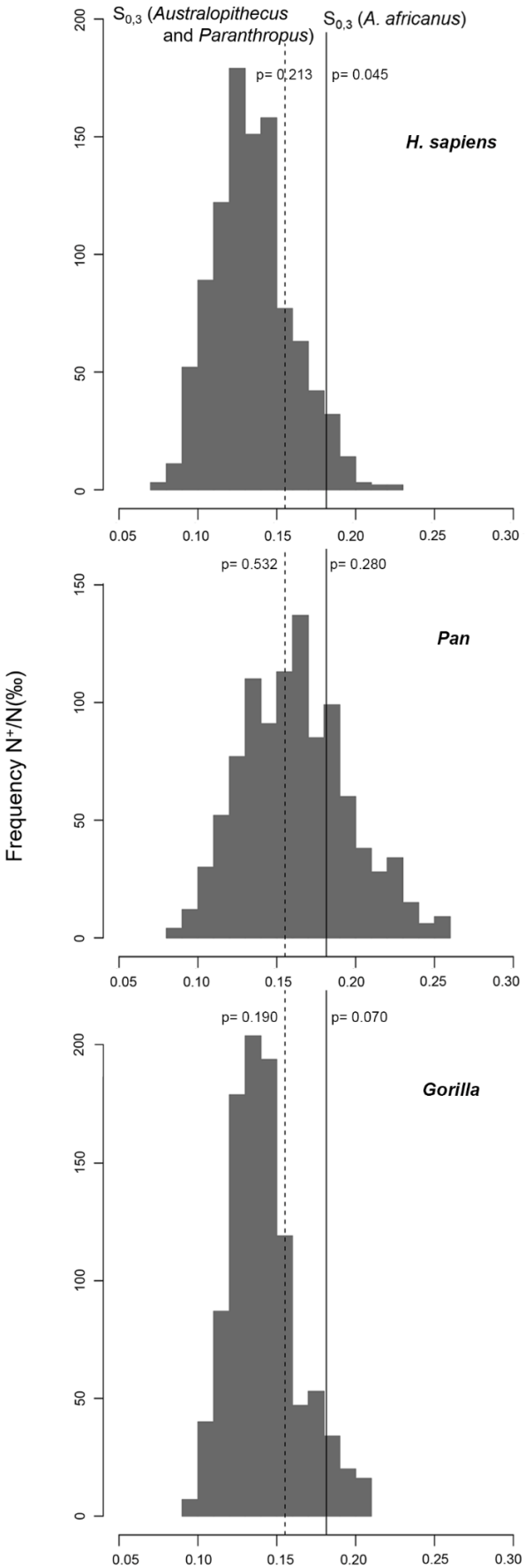

Fig. S6. Histograms of phenetic distances of *A. africanus* (black line) and combined A.L. 288-1, U.W. 88-98 and TM1517 (dashed line) with *H. sapiens*, *Pan* and *Gorilla* using the Procrustes shape coordinates of combined trochlea and medial malleolar.

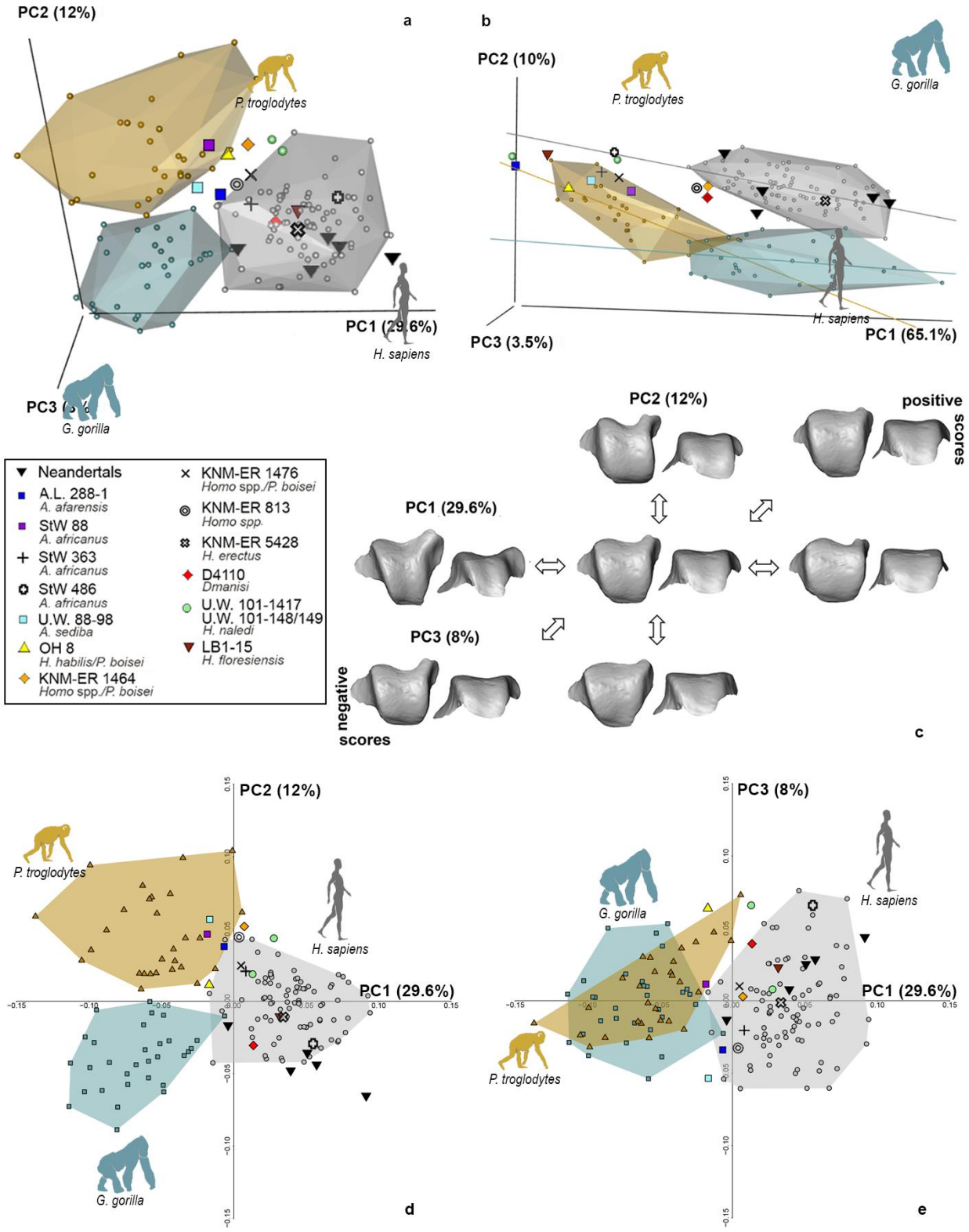

Fig. S7. Combined trochlea, medial and lateral malleolar facets. PCA plot of the trochlea, medial and lateral malleolar facets in shape space (a) and in form space (b). Shape changes along the first three PC axes (c) in dorsal (left) and posterior (right) views. 2D PCA depicting PC1 vs. PC2 (d) and PC1 vs. PC3 (e).

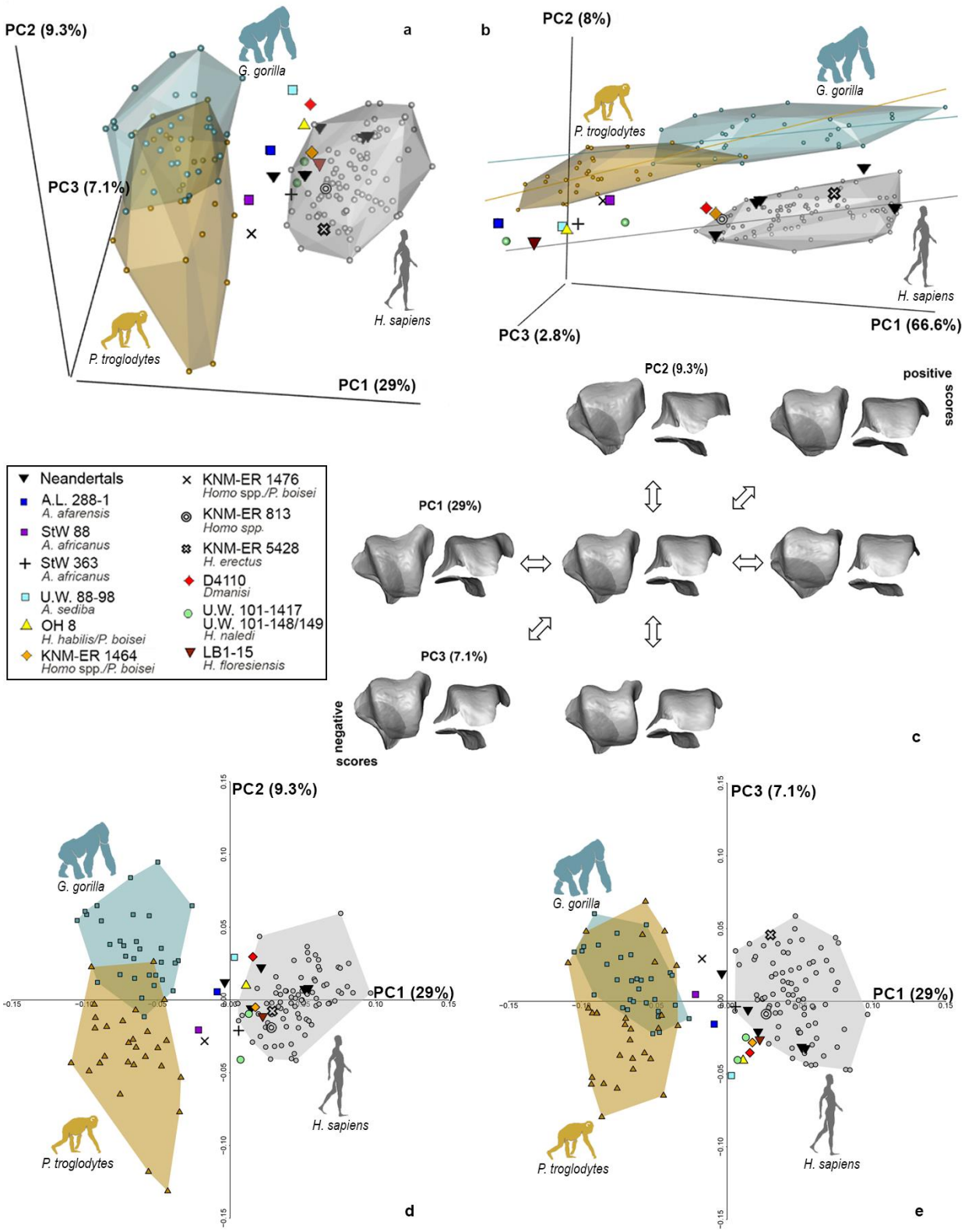

Fig. S8. Combined posterior calcaneal facet, trochlea, medial and lateral malleolar facets. PCA plot of the combined posterior calcaneal facet, trochlea, medial and lateral malleolar facets in shape space (a) and in form space (b). Shape changes along the first three PC axes (c) in dorsal (left) and posterior (right) views. 2D PCA depicting PC1 vs. PC2 (d) and PC1 vs. PC3 (e).

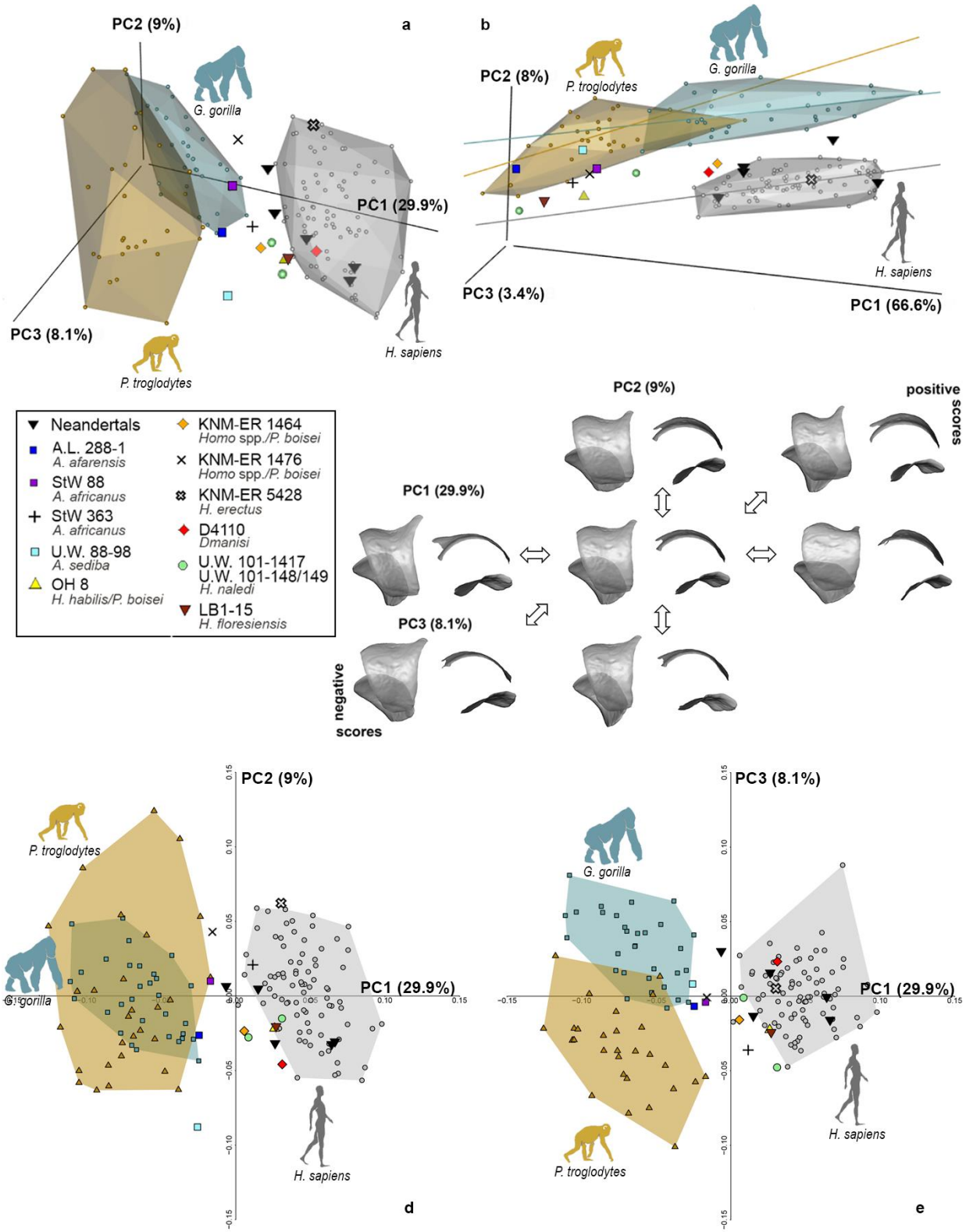

Fig. S9. Combined posterior calcaneal facet and trochlea. PCA plot of the combined posterior calcaneal facet and trochlea in shape space (a) and in form space (b). Shape changes along the first three PC axes (c) in dorsal (left) and lateral (right) views. 2D PCA depicting PC1 vs. PC2 (d) and PC1 vs. PC3 (e).

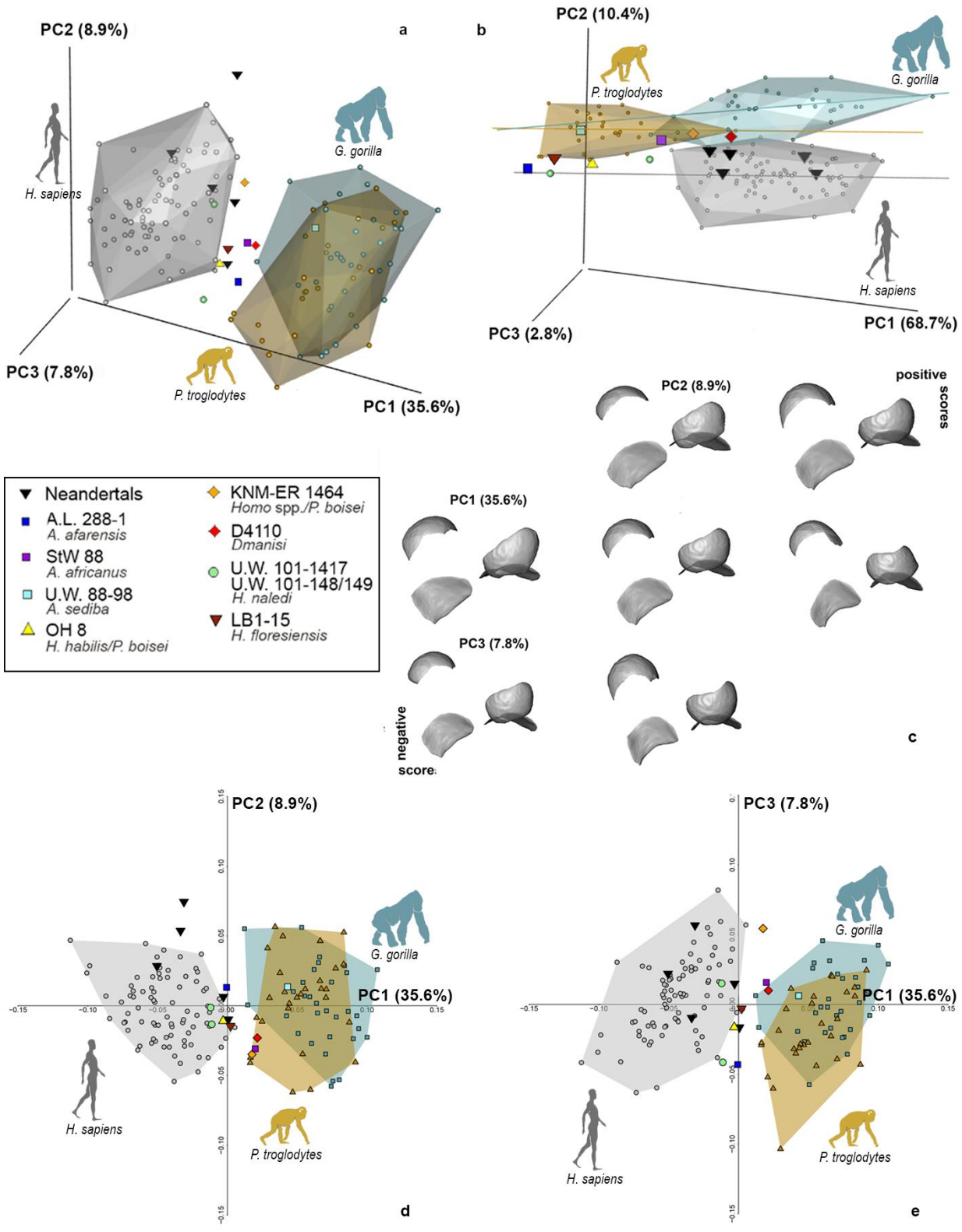

Fig. S10. Combined navicular and posterior calcaneus facets. PCA plot of the combined navicular and posterior calcaneus facets in shape space (a) and in form space (b). Shape changes along the first three PC axes (c) in plantar (left) and frontal (right) views. 2D PCA depicting PC1 vs. PC2 (d) and PC1 vs. PC3 (e).

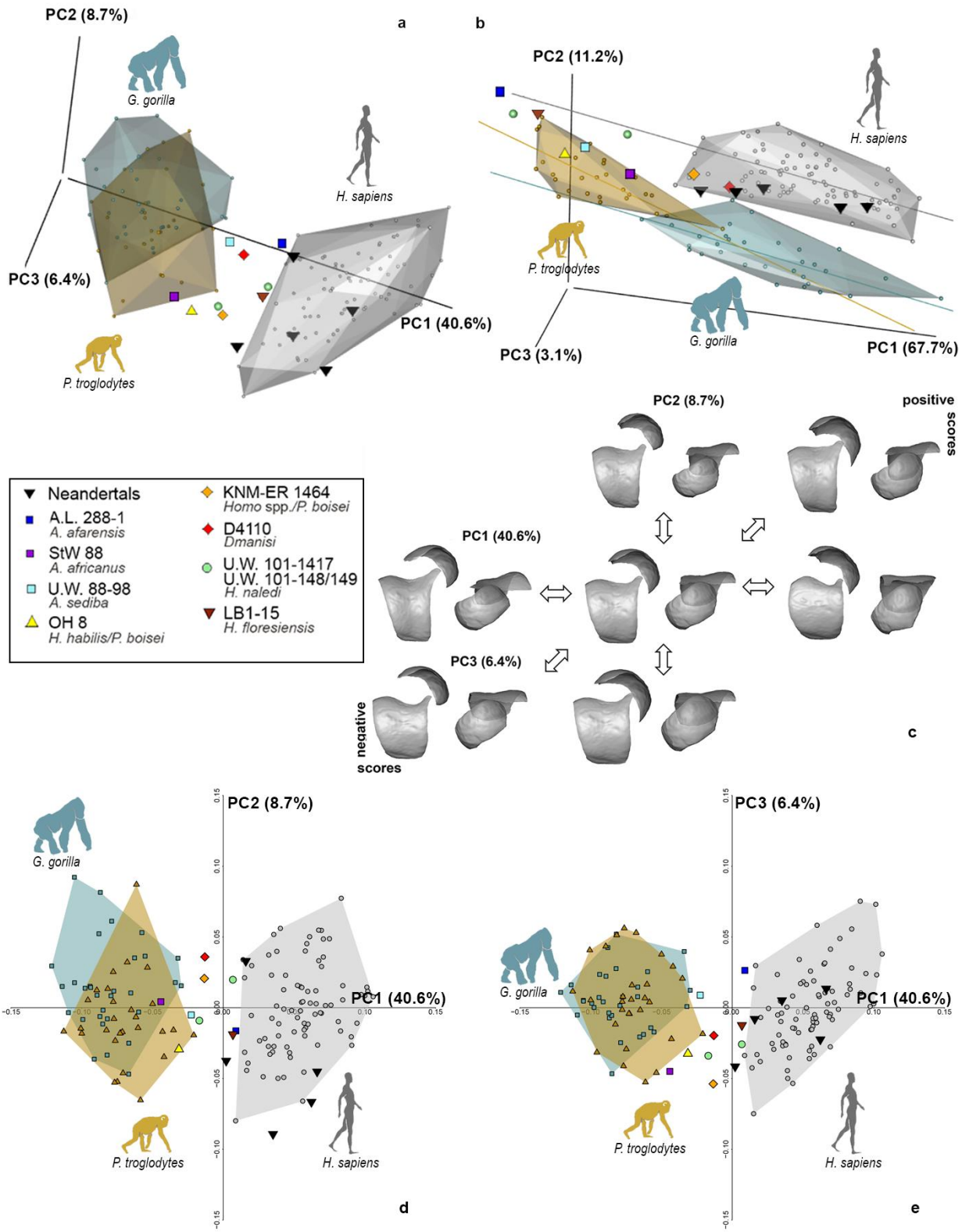

Fig. S11. Combined navicular facet and trochlea. PCA plot of the combined navicular facet and trochlea in shape space (a) and in form space (b). Shape changes along the first three PC axes (c) in dorsal (left) and frontal (right) views. 2D PCA depicting PC1 vs. PC2 (d) and PC1 vs. PC3 (e).

Table S1. Extant sample.

Sample	Sample size	Collections[a]
H. sapiens		
UP-LSA[b]	5	DBP, NHMP
Medieval	3	DBC
Roccapelago	15	SAPAB
Norris Farms	5	ISM
Native Americans	8	PAHM
Bologna	39	BiGeA
Nguni	6	BiGeA
Gorilla		
Gorilla gorilla	31	NHM, PCM, UCL, NMNH, CMNH
Pan		
Pan troglodytes	29	NHM, PCM, UCL, NMNH, CMNH

[a]DBP, Department of Biology, University of Pisa, Pisa; NHMP, The Natural History Museum, Department of Earth Sciences, London; DBC, Department of Cultural Heritage, University of Bologna, Ravenna; SAPAB, Soprintendenza Archeologia, Belle Arti e Paesaggio per la città metropolitana di Bologna e le province di Modena, Ferrara e Reggio Emilia; ISM, Illinois State Museum, Springfield; PAHM, P. A. Hearst Museum Collections, University of California, Berkeley; BiGeA, Department of Biological, Geological and Environmental Sciences, University of Bologna, Bologna; NHM, Natural History Museum London, Mammals collection, London; PCM, Powell Cotton Museum, Birchington, Kent; UCL, Anthropology Department Napier Collection, University College London; NMNH, National Museum of Natural History, Smithsonian, Washington; CMNH, Cleveland Museum of Natural History, Cleveland.
[b]UP, Upper Paleolithic (Romito 7, Romito 8, Romito 9 and Veneri 2); LSA, Late Stone Age (Clark Howell Omo, Ethiopia).

Table S2. Extinct hominin sample.

Specimens	Taxon designation	Date	Main references for fossils listed
A.L. 288-1	*A. afarensis*	3.18 Ma	Prang, 2016; Boyer et al., 2015; Boyle and DeSilva, 2015; Harcourt-Smith et al., 2015; Prang, 2015; Parr et al., 2011; Zipfel et al., 2011; Pontzer et al., 2010; Jungers et al., 2009; DeSilva, 2008; Gebo and Schwartz, 2006; Harcourt-Smith, 2002; Latimer et al., 1987; Lamy, 1986; Stern and Susman, 1983.
StW 363	*A. africanus*	2.0-2.6 Ma	Harcourt-Smith et al., 2015; Boyle and DeSilva, 2015; Prang, 2015; Zipfel et al., 2011; DeSilva, 2008; Harcourt-Smith, 2002.
StW 486	*A. africanus*	2.0-2.6 Ma	Boyle and DeSilva, 2015; Zipfel et al., 2011; DeSilva, 2008.
StW 88	*A. africanus*	2.0-2.6 Ma	Prang, 2016; Boyle and DeSilva, 2015; Prang, 2015; Harcourt-Smith et al., 2015; Zipfel et al., 2011; Jungers et al., 2009; DeSilva, 2008; Harcourt-Smith, 2002.
U.W. 88-98	*A. sediba*	1.97 Ma	Prang, 2016; Boyle and DeSilva, 2015; Harcourt-Smith et al., 2015; Prang, 2015; DeSilva et al., 2013; Zipfel et al., 2011.
TM 1517	*P. robustus*	1.9 - 2.0 Ma	Prang, 2016; Boyle and DeSilva, 2015; Harcourt-Smith et al., 2015; Zipfel et al., 2011; DeSilva, 2008; Gebo and Schwartz, 2006; Harcourt-Smith, 2002.
OH 8	*H. habilis/P. boisei?*	1.8 Ma	Prang, 2016; Boyer et al., 2015; Boyle and DeSilva, 2015; Harcourt-Smith et al., 2015; Prang, 2015; Parr et al., 2011; Zipfel et al., 2011; Pontzer et al., 2010; Jungers et al., 2009; DeSilva, 2008; Gebo and Schwartz, 2006; Harcourt-Smith, 2002; Lamy, 1986; Oxnard and Lisowski, 1980; Day and Wood, 1968; Day and Napier, 1964.
KNM-ER 1464	*Homo* spp./*P. boisei?*	1.7 Ma	Prang, 2016; Boyer et al., 2015; Boyle and DeSilva, 2015; Harcourt-Smith et al., 2015; Prang, 2015; Su et al., 2013; Parr et al., 2011; Zipfel et al., 2011; Pontzer et al., 2010; Jungers et al., 2009; DeSilva, 2008; Gebo and Schwartz, 2006; Harcourt-Smith, 2002; Lamy, 1986.
KNM-ER 1476	*Homo* spp./*P. boisei?*	1.88 Ma	Prang, 2016; Boyle and DeSilva, 2015; Harcourt-Smith et al., 2015; Parr et al., 2011; Zipfel et al., 2011; Pontzer et al., 2010; Jungers et al., 2009; DeSilva, 2008; Gebo and Schwartz, 2006; Harcourt-Smith, 2002; Lamy, 1986.
KNM-ER 813	*Homo* spp.	1.85 Ma	Prang, 2016; Boyer et al., 2015; Boyle and DeSilva, 2015; Prang, 2015; Harcourt-Smith et al., 2015; Zipfel et al., 2011; Pontzer et al., 2010; Jungers et al., 2009; DeSilva, 2008; Gebo and Schwartz, 2006; Harcourt-Smith, 2002; Lamy, 1986.
KNM-ER 5428	*H. erectus*	1.6 Ma	Prang, 2016; Boyle and DeSilva, 2015; Harcourt-Smith et al., 2015; Prang, 2015; Zipfel et al., 2011; DeSilva, 2008.
D4110 (Dmanisi)	*H. erectus*	1.77 Ma	Pontzer et al., 2010.
U.W. 101-148/149	*H. naledi*	236 - 335 Ka	Harcourt-Smith et al., 2015.
U.W. 101-1417	*H. naledi*	236 - 335 Ka	Harcourt-Smith et al., 2015.
LB1-15	*H. floresiensis*	60-100 Ka	Prang, 2016; Harcourt-Smith et al., 2015; Prang, 2015; Jungers et al., 2009; Sutikna et al., 2016.
Ferrassie 1	*H. neanderthalensis*	43 - 45 Ka	Boyle and DeSilva, 2015; Jungers et al., 2009; Trinkaus, 1983; Rhoads and Trinkaus, 1977.
Ferrassie 2	*H. neanderthalensis*	43 - 45 Ka	Boyle & DeSilva, 2015; Boyle and DeSilva, 2015; Trinkaus, 1983; Rhoads and Trinkaus, 1977.
SP4B (Spy 2	*H. neanderthalensis*	ca. 36 Ka	Parr et al., 2011; Trinkaus, 1983; Rhoads and Trinkaus, 1977.
EM 3519 (Tabun C1	*H. neanderthalensis*	122±16 Ka	Boyle and DeSilva, 2015; Parr et al., 2011; Trinkaus, 1983; Rhoads and Trinkaus, 1977.
Krapina 235	*H. neanderthalensis*	130 Ka	Rhoads and Trinkaus, 1977.

Table S3. Number and percentages of estimated (semi)landmarks for singular and combined facets[a].

Specimens	Shape[b]	NF	AMCF	TF	PCF	MMF	LMF	TF-NF	PCF-NF	PCF-TF	TF-PCF-NF	TF-LMF	TF-MMF	TF-LMF-MMF	TF-PCF-LMF-MMF
A.L. 288-1	0	0	0	0	0	0	0	0	0	0	0	0	0	0	0
StW 363	-	-	-	5 (10.4%)	11 (26.2%)	0	8 (24.2%)	-	-	16 (17.8%)	-	13 (18.1%)	5 (8.3%)	13 (15.5%)	24 (19%)
StW 486	-	-	-	15 (31.3%)	-	4 (19%)	0	-	-	-	-	13 (18.1%)	17 (28.3%)	17 (28.3%)	-
StW 88	22 (8.8%)	13 (31.7%)	3 (13%)	0	0	0	0	13 (14.6%)	13 (15.7%)	0	13 (9.9%)	0	0	0	0
U.W. 88-98	0	0	0	0	0	0	0	0	0	0	0	0	0	0	0
TM 1517	-	-	-	14 (29.2%)	-	0	-	-	-	-	-	-	14 (23.3%)	-	-
OH 8	29 (11.6%)	0	0	0	14 (33.3%)	0	2 (6.1%)	0	14 (16.9%)	14 (15.6%)	14 (10.7%)	2 (2.8%)	0	2 (2.4%)	16 (12.7%)
KNM-ER 813	-	-	-	7 (14.6%)	14 (33.3)	0	7 (21.2%)	-	-	21 (23.3%)	-	14 (9.4%)	7 (11.7%)	14 (16.7%)	28 (22.2%)
KNM-ER 1464	0	0	0	0	0	0	0	0	0	0	0	0	0	0	0
KNM-ER 1476	-	-	-	0	0	0	0	-	-	0	-	0	0	0	0
D4110	13 (5.2%)	4 (9.8)	3 (13%)	0	2 (4.8%)	0	0	4 (4.5%)	4 (4.9%)	0	4 (3.1%)	0	0	0	0
KNM-ER 5428	-	-	-	10 (20.8%)	15 (35.7%)	1 (4.8%)	3 (9.1%)	-	-	10 (11.1%)	-	13 (18.1%)	11 (18.3%)	14 (16.7%)	14 (11.1%)
U.W. 101-148/149	26 (10.4%)	7 (17.1%)	0	1 (2.1%)	4 (9.5%)	0	0	8 (9%)	11 (13.3%)	5 (5.6%)	12 (9.2%)	1 (1.4%)	1 (1.7%)	1 (1.2%)	5 (4%)
U.W. 101-1417	18 (7.2%)	6 (14.6%)	3 (13%)	1 (2.1%)	0	0	0	7 (7.9%)	6 (7.2%)	1 (1.1%)	7 (5.3%)	1 (1.4%)	1 (1.7%)	1 (1.2%)	1 (0.8%)
LB1-15	8 (3.2)	7 (17.1%)	1 (4.3%)	0	0	0	0	7 (7.9%)	7 (8.4%)	0	7 (5.3%)	0	0	0	0
Ferrassie 1	0	0	0	0	0	0	0	0	0	0	0	0	0	0	0
Ferrassie 2	0	0	0	0	0	0	0	0	0	0	0	0	0	0	0
SP4B	0	0	0	0	0	0	0	0	0	0	0	0	0	0	0
EM 3519	0	0	0	0	0	0	0	0	0	0	0	0	0	0	0
Krapina 235	21 (8.4)	1 (2.4%)	0	4 (8.3%)	0	0	4 (12.1%)	5 (%.6%)	1 (1.2%)	4 (4.4%)	5 (3.8%)	8 (11.1%)	4 (6.7%)	8 (9.5%)	8 (6.4%)

[a]List of acronyms used: NF, navicular facet; AMCF, anterior and medial calcaneal facets; TF, trochlea facet; PCF, posterior calcaneal facet; MML, medial malleolar facet; LMF, lateral malleolar facet; TF-NF, combined trochlea and navicular facets; PCF-NF, combined posterior calcaneal facet and navicular facets; PCF-TF, combined posterior calcaneal facet and trochlea facets; TF-PCF-NF, combined trochlea, posterior calcaneal and navicular facets; TF-LMF, combined trochlea and lateral malleolar facets; TF-MMF, combined trochlea and medial malleolar facets; TF-LMF-MMF, combined trochlea, lateral and medial malleolar facets; TF-PCF-LMF-MMF, combined trochlea, posterior calcaneal, lateral and medial malleolar facets.

[b]Shape includes also (semi)landmarks of flexor hallucis longus groove and neck surface.

Table S4. P-values for post hoc (ANOVA) comparisons of shape space scores of PCs (1-3) among extant taxa.

	PC1			PC2			PC3		
Variable	*H. sapiens*	*Pan*	*Gorilla*	*H. sapiens*	*Pan*	*Gorilla*	*H. sapiens*	*Pan*	*Gorilla*
Talus									
Homo sapiens	x	0.000*	0.000*	x	0.000*	0.000*	x	0.02*	0.937
Pan		x	0.162		x	0.000*		x	0.117
Gorilla			x			x			x
Navicular facet									
Homo sapiens	x	0.000*	0.000*	x	0.089	0.828	x	0.000*	0.621
Pan		x	0.982		x	0.065		x	0.000*
Gorilla			x			x			x
Trochlea									
Homo sapiens	x	0.000*	0.000*	x	0.000*	0.000*	x	0.003*	0.034*
Pan		x	0.590		x	0.000*		x	0.000*
Gorilla			x			x			x
Posterior calcaneal facet									
Homo sapiens	x	0.000*	0.000*	x	0.004*	0.996	x	0.000*	0.000*
Pan		x	0.901		x	0.000*		x	0.000*
Gorilla			x			x			x
Anterior-medial calcaneal facet									
Homo sapiens	x	0.000*	0.197	x	0.000*	0.000*	x	0.018*	0.984
Pan		x	0.001*		x	0.664		x	0.080
Gorilla			x			x			x
Medial malleolar facet									
Homo sapiens	x	0.000*	0.000*	x	0.000*	0.983	x	0.000*	0.225
Pan		x	0.000*		x	0.000*		x	0.000*
Gorilla			x			x			x
Lateral malleolar facet									
Homo sapiens	x	0.000*	0.000*	x	0.000*	0.000*	x	0.347	0.050
Pan		x	0.573		x	0.992		x	0.006*
Gorilla			x			x			x
Trochlea and navicular facet									
Homo sapiens	x	0.000*	0.000*	x	0.340	0.087	x	0.570	0.520
Pan		x	0.199		x	0.011*		x	0.998
Gorilla			x			x			x
Posterior calcaneal and navicular facets									
Homo sapiens	x	0.000*	0.000*	x	0.000*	0.791	x	0.386	0.962
Pan		x	0.026*		x	0.019*		x	0.648
Gorilla			x			x			x
Trochlea and posterior calcaneal facet									
Homo sapiens	x	0.000*	0.000*	x	0.707	0.748	x	0.000*	0.000*
Pan		x	0.161		x	0.997		x	0.000*
Gorilla			x			x			x
Trochlea, posterior calcaneal and navicular facets									
Homo sapiens	x	0.000*	0.000*	x	0.008*	0.025*	x	0.000*	0.432
Pan		x	79,000		x	0.000*		x	0.000*
Gorilla			x			x			x
Trochlea and medial malleolar facet									
Homo sapiens	x	0.000*	0.000*	x	0.000*	0.000*	x	0.516	0.111
Pan		x	0.227		x	0.000*		x	0.029*
Gorilla			x			x			x
Trochlea and lateral malleolar facet									
Homo sapiens	x	0.000*	0.000*	x	0.000*	0.000*	x	0.188	0.533
Pan		x	0.929		x	0.000*		x	0.823
Gorilla			x			x			x
Trochlea, medial and lateral malleolar facets									
Homo sapiens	x	0.000*	0.000*	x	0.000*	0.000*	x	0.118	0.788
Pan		x	0.180		x	0.000*		x	0.497
Gorilla			x			x			x
Trochlea, posterior calcaneal, medial and lateral malleolar facets									
Homo sapiens	x	0.000*	0.000*	x	0.000*	0.000*	x	0.032*	0.169
Pan		x	0.686		x	0.000*		x	0.045*
Gorilla			x			x			x

*Significant P-value (P = < 0.05).

Supplementary references

Boyer, D.M., Yapuncich, G.S., Butler, J.E., Dunn, R.H., Seiffert, E.R., 2015. Evolution of postural diversity in primates as reflected by the size and shape of the medial tibial facet of the talus. American Journal of Physical Anthropology 157, 134-177.

Boyle, E., DeSilva, J.M., 2015. A large *Homo erectus* talus from Koobi Fora, Kenya (KNM-ER 5428), and Pleistocene hominin talar evolution. PaleoAnthropology 2015, 1–13.

Day, M. H., Napier, J.R., 1964. Hominid fossils from Bed I, Olduvai Gorge, Tanganyika: fossil foot bones. Nature 201, 967.

Day, M. H., Wood, B.A., 1968. Functional affinities of the Olduvai Hominid 8 talus. Man. 3, 440–455.

DeSilva, J.M., 2008. Vertical climbing adaptations in the anthropoid ankle and midfoot: implications for locomotion in Miocene catarrhines and Plio-Pleistocene hominins. Ph.D. Dissertation, The University of Michigan.

DeSilva, J.M., Holt, K.G., Churchill, S.E., Carlson, K.J., Walker, C.S., Zipfel, B., Berger, L.R., 2013. The lower limb and mechanics of walking in A*ustralopithecus sediba*. Science 340, 1232999.

DeSilva J.M., Bonne-Annee, R., Swanson, Z., Gill, C.M., Sobel, M., Uy, J., Gill, S.V., 2015. Midtarsal break variation in modern humans: functional causes, skeletal correlates, and paleontological implications. American Journal of Physical Anthropology 156, 543–552.

Gebo, D.L., Schwartz, G.T., 2006. Foot bones from Omo : implications for hominid evolution. American Journal of Physical Anthropology 129, 499–511.

Harcourt-Smith, W.E.H., 2002. Form and function in the hominoid tarsal skeleton. Ph.D. Dissertation, University of London.

Harcourt-Smith, W.H.E., Throckmorton, Z., Congdon, K.A., Zipfel, B., Deane, A.S., Drapeau, M.S.M., Churchill, S.E., Berger, L.R., Desilva, J.M., 2015. The foot of *Homo naledi*. Nature Communications 6, 1–8.

Jungers, W.L., Harcourt-Smith, W.E.H., Wunderlich, R.E., Tocheri, M.W., Larson, S.G., Sutikna, T., Due, R.A., Morwood, M.J., 2009. The foot of *Homo floresiensis*. Nature 459, 81–84.

Lamy, P., 1986. The settlement of the longitudinal plantar arch of some African Plio-Pleistocene hominids: a morphological study. Journal of Human Evolution 15, 31–46.

Latimer, B., Ohman, J.C., Lovejoy, C.O., 1987. Talocrural joint in African hominoids: implications for *Australopithecus afarensis*. American Journal of Physical Anthropology 74, 155–175.

Oxnard, C.E., Lisowski, P.F., 1980. Functional articulation of some hominoid foot bones: implications for the Olduvai (Hominid 8) foot. American Journal of Physical Anthropology 52, 107–117.

Parr, W.C.H., Chatterjee, H.J., Soligo, C., 2011. Inter- and intra-specific scaling of articular surface areas in the hominoid talus. Journal of Anatomy 218, 386–401.

Pontzer, H., Rolian, C., Rightmire, G.P., Jashashvili, T., Ponce de León, M.S., Lordkipanidze, D., Zollikofer, C.P.E., 2010. Locomotor anatomy and biomechanics of the Dmanisi hominins. Journal of Human Evolution 58, 492–504.

Prang, T.C., 2015. Rearfoot posture of A*ustralopithecus sediba* and the evolution of the hominin longitudinal arch. Scientific reports 5, 17677.

Prang, T.C., 2016. The subtalar joint complex of *Australopithecus sediba*. Journal of Human Evolution 90, 105–119.

Rhoads, J.G., Trinkaus, E., 1977. Morphometrics of the Neandertal talus. American journal of physical anthropology 46, 29–43.

Stern, J.T., Susman, R.L., 1983. The locomotor anatomy of *Australopithecus afarensis*. American Journal of Physical Anthropology 60, 279–317.

Su, A., Wallace, I.J., Nakatsukasa, M., 2013. Trabecular bone anisotropy and orientation in an Early Pleistocene hominin talus from East Turkana , Kenya. Journal of Human Evolution 64, 667–677.

Sutikna, T., Tocheri, M.W., Morwood, M.J., Saptomo, E.W., Jatmiko, Awe, R.D., Wasisto, S., Westaway, K.E., Aubert, M., Li, B., Zhao, J.X., Storey, M., Alloway, B. V., Morley, M.W., Meijer, H.J.M., Van Den Bergh, G.D., Grün, R., Dosseto, A., Brumm, A., Jungers, W.L., Roberts, R.G., 2016. Revised stratigraphy and chronology for *Homo floresiensis* at Liang Bua in Indonesia. Nature 532, 366–369.

Trinkaus, E., 1983. Functional aspects of Neandertal pedal remains. Foot & Ankle 3, 377–390.

Zipfel, B., DeSilva, J.M., Kidd, R.S., Carlson, K.J., Churchill, S.E., Berger, L.R., 2011. The foot and ankle of *Australopithecus sediba*. Science 333, 1417–1420.